HOKKAIDO UNIVERSITY

Title	Crustal magma pathway beneath Aso caldera inferred from three-dimensional electrical resistivity structure
Author(s)	Hata, Maki; Takakura, Shinichi; Matsushima, Nobuo; Hashimoto, Takeshi; Utsugi, Mitsuru
Citation	Geophysical Research Letters, 43(20), 10,720-10,727 https://doi.org/10.1002/2016GL070315
Issue Date	2016-10-28
Doc URL	http://hdl.handle.net/2115/65174
Rights	An edited version of this paper was published by AGU. Copyright 2016 American Geophysical Union. Hata, M., S. Takakura, N. Matsushima, T. Hashimoto, and M. Utsugi, (2016), Crustal magma pathway beneath Asocaldera inferred from three-dimensional electrical resistivity structure, Geophys. Res. Lett., 43, 10,720–10,727, doi:10.1002/2016GL070315. To view the published open abstract, go to http://dx.doi.org and enter the DOI.
Type	article
File Information	Hata_et_al_2016_GRL.pdf

Instructions for use

Hokkaido University Collection of Scholarly and Academic Papers : HUSCAP

AGU PUBLICATIONS

Geophysical Research Letters

RESEARCH LETTER
10.1002/2016GL070315

Key Points:
- Magmatic eruption occurs cyclically at Naka-dake first crater in Aso caldera
- Three-dimensional electrical resistivity structure reveals a stable magma pathway/reservoir in the crust
- Earthquake clusters are distributed at the resistive sides along the upper surface of the inferred magma reservoir

Supporting Information:
- Supporting Information S1

Correspondence to:
M. Hata,
m.hata@aist.go.jp

Citation:
Hata, M., S. Takakura, N. Matsushima, T. Hashimoto, and M. Utsugi (2016), Crustal magma pathway beneath Aso caldera inferred from three-dimensional electrical resistivity structure, *Geophys. Res. Lett.*, *43*, 10,720–10,727, doi:10.1002/2016GL070315.

Received 5 JUL 2016
Accepted 11 OCT 2016
Accepted article online 13 OCT 2016
Published online 28 OCT 2016

©2016. American Geophysical Union. All Rights Reserved.

Crustal magma pathway beneath Aso caldera inferred from three-dimensional electrical resistivity structure

Maki Hata[1], Shinichi Takakura[1], Nobuo Matsushima[1], Takeshi Hashimoto[2], and Mitsuru Utsugi[3]

[1]National Institute of Advanced Industrial Science and Technology, Tsukuba, Japan, [2]Institute of Seismology and Volcanology, Faculty of Science, Hokkaido University, Sapporo, Japan, [3]Aso Volcanological Laboratory, Institute for Geothermal Sciences, Graduate School of Science, Kyoto University, Kumamoto, Japan

Abstract At Naka-dake cone, Aso caldera, Japan, volcanic activity is raised cyclically, an example of which was a phreatomagmatic eruption in September 2015. Using a three-dimensional model of electrical resistivity, we identify a magma pathway from a series of northward dipping conductive anomalies in the upper crust beneath the caldera. Our resistivity model was created from magnetotelluric measurements conducted in November–December 2015; thus, it provides the latest information about magma reservoir geometry beneath the caldera. The center of the conductive anomalies shifts from the north of Naka-dake at depths >10 km toward Naka-dake, along with a decrease in anomaly depths. The melt fraction is estimated at 13–15% at ~2 km depth. Moreover, these anomalies are spatially correlated with the locations of earthquake clusters, which are distributed within resistive blocks on the conductive anomalies in the northwest of Naka-dake but distributed at the resistive sides of resistivity boundaries in the northeast.

1. Introduction

Aso, on the island of Kyushu in the Southwest Japan Arc (Figure 1), is one of the world's largest calderas, with a diameter of up to 25 km. The caldera was formed during 270–90 ka by four huge eruptions that produced hundreds of cubic kilometers of pyroclastic deposits [e.g., *Matsumoto et al*., 1991; *Ono et al*., 1977]. Subsequently, a number of postcaldera cones/volcanoes formed in the central part of the caldera. Naka-dake (Figure 1a), which is a complex stratovolcano consisting of basaltic andesite and andesite, has erupted since the sixth century. Volcanic eruptions at Aso caldera have occurred only at Naka-dake's northernmost crater (the first crater) since 1933. Besides Aso, some of the world's largest calderas, including Aira Caldera, and numerous active Quaternary volcanoes, including Sakurajima, Kirishima, and Kuju volcanoes, are present in Kyushu along the volcanic front related to subduction of the Philippine Sea Plate.

The surface activity at Naka-dake's first crater is well known as a cyclical system comprising three main states: (1) in the quietest state, the crater fills with a large amount of hot acidic water; (2) in the intermediate state, thermal energy dries the crater lake and incandescent phenomena occur on the crater wall and floor; and (3) in the most active state, the crater experiences Strombolian eruptions [e.g., *Sudo*, 2001]. A recent magmatic eruption occurred in November 2014 after 22 years of quiescence, a phreatomagmatic eruption (the first in 21 years) occurred in September 2015, and an explosive eruption (the first in 27 years) occurred in October 2016 with spewing volcanic ash 11,000 m into the air. Prior to the eruptive activity, incandescent phenomena were observed in 2000, mud eruptions occurred during 2003–2004 following a sharp reduction of the water level of the crater lake, the disappearance and appearance of crater lakes were repeated after that, and small phreatic eruptions were observed after 2011. Subsequently, the crater lake dried up gradually beginning in mid-2013, at which time volcanic activity began to increase. Thus, Naka-dake is considered to keep an active state for the past 15 years.

The crustal structure beneath Aso caldera has been studied previously by electromagnetic and seismic surveys. Seismic tomography of the crust has identified low-velocity anomalies beneath the caldera that may correspond to magma chambers [e.g., *Sudo and Kong*, 2001; *Abe et al*., 2010]. *Sudo and Kong* [2001] reported a spherical low-velocity anomaly centered at 6 km depth that flattens at 10 km depth to the west of Naka-dake (Figure 1). *Abe et al*. [2010] reported a large, low *S* wave velocity layer at a depth of about 17 km, corresponding to the Conrad discontinuity in and around Aso caldera. These low-velocity anomalies are thought to represent a magma chamber with a total volume of about 100 km^3. Additionally,

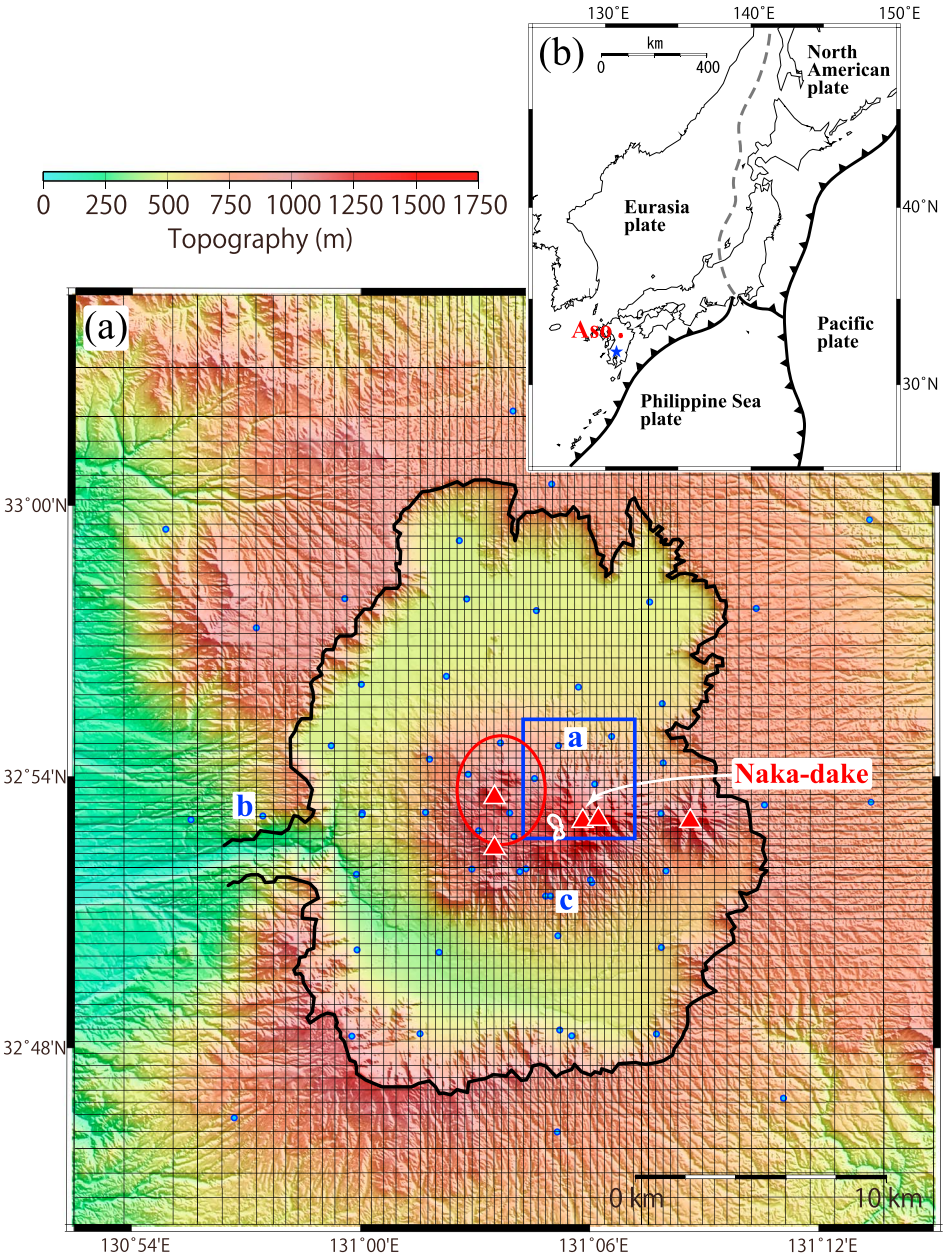

Figure 1. (a) Topographic map around Aso caldera showing 55 magnetotelluric (MT) sites (blue dots). Red triangles, white outline, and black outline indicate the five main postcaldera cones, Naka-dake first crater, and the rim of Aso caldera, respectively. The blue rectangle and red circle indicate an inferred sill-like deformation source at a depth of 15.5 km [*Geographical Survey Institute*, 2004] and a spherical *P* velocity anomaly of $< -15\%$ at a depth of 6 km [*Sudo and Kong*, 2001]. Black lines represent grids in the three-dimensional inversion. Three sites, labeled a, b, and c, indicate the representative sites used for sounding curves in Figure 2. (b) Location of Aso caldera (red square) on the island of Kyushu in the Japan Arc, with plate boundaries indicated by lines and triangles indicating the direction of motion for each plate. Blue star indicates the location of the remote reference site used in this study.

Geographical Survey Institute [2004] reported a sill-like deformation source inferred from GPS data at a depth of 15.5 km beneath the caldera (Figure 1). Despite these promising seismic studies, the resolution of electrical resistivity structures has been limited to depths shallower than about 5 km to focus on shallow structure around the volcanic cones in the central part of the caldera [e.g., *Hase et al.*, 2005; *Kanda et al.*, 2008]. Studies of larger-scale ($>$10 km to several tens of kilometers) resistivity structures have reported that the crust and upper mantle beneath Aso caldera are relatively resistive compared with those beneath the other

subduction volcanoes in Kyushu [e.g., *Handa*, 2005; *Hata et al*., 2015]. However, the fine-scale (<10 km) resistivity structure of the crust beneath Aso caldera remains unknown. Thus, further electromagnetic investigation is required to assess the possible distributions of magma pathways and reservoirs. In this study, we examine the electrical resistivity structure at depths of <20 km beneath Aso caldera, using a three-dimensional inversion procedure.

2. Method

2.1. MT Surveys and Data

Electromagnetic soundings, including magnetotelluric (MT) surveys, are highly sensitive to even a few percent fluid (aqueous fluid and/or melt), especially when fluids are interconnected [e.g., *Hyndman and Shearer*, 1989]. Thus, MT methods are considered an important technique for detecting magma reservoirs. We carried out an MT survey across Aso caldera from November to December 2015 using *Phoenix Geophysics Ltd*. MTU-5A systems and obtained five-component electromagnetic data at 55 sites. MT sites were arranged with a spacing of ~5 km, as shown in Figure 1a. Sites were more densely concentrated around volcanic cones. The area immediately around the first crater could not be investigated, due to a restricted access zone (2 km radius) imposed by the Aso Volcano Disaster Prevention Council. Data were recorded for 14 h, between 6 P.M. and 8 A.M. on the following day, at sampling intervals of 15 Hz or 2400 Hz (0.067 s or 0.00042 s), then remote referenced against a site located 100 km from Aso caldera (Figure 1b). We used six MT response functions, $\mathbf{Z}(\mathbf{r}, T)$ and $\mathbf{T}(\mathbf{r}, T)$, at periods ranging from 0.005 to 2380 s, to invert for resistivity structure in three dimensions; $\mathbf{Z}(\mathbf{r}, T)$ and $\mathbf{T}(\mathbf{r}, T)$ are called the MT impedance and tipper, respectively [e.g., *Cagniard*, 1953]. The four components of the MT impedance tensor and the two components of the tipper vector are given by

$$\begin{pmatrix} E_X(\mathbf{r}, T) \\ E_Y(\mathbf{r}, T) \\ H_Z(\mathbf{r}, T) \end{pmatrix} = \begin{pmatrix} Z_{XX}(\mathbf{r}, T) & Z_{XY}(\mathbf{r}, T) \\ Z_{YX}(\mathbf{r}, T) & Z_{YY}(\mathbf{r}, T) \\ T_{ZX}(\mathbf{r}, T) & T_{ZY}(\mathbf{r}, T) \end{pmatrix} \begin{pmatrix} H_X(\mathbf{r}, T) \\ H_Y(\mathbf{r}, T) \end{pmatrix}, \quad (1)$$

where $\mathbf{r}$ denotes the site location, T denotes the period, $E_X(\mathbf{r}, T)$ and $E_Y(\mathbf{r}, T)$ denote the horizontal components of the electric field, and $H_X(\mathbf{r}, T)$, $H_Y(\mathbf{r}, T)$, and $H_Z(\mathbf{r}, T)$ denote the horizontal and vertical components of the magnetic field.

2.2. Electrical Resistivity Modeling

We performed a three-dimensional inversion for crustal-scale electrical resistivity structure using the six MT response functions for 55 sites with good signal-to-noise ratios. A parallel array of Intel Xeon™ CPUs, comprising 28 processors with 512 Gb memory, was used for the inversion procedure. The inversion used a parallel-optimized DASOCC code that applied a data space method to reduce computation time [*Siripunvaraporn and Egbert*, 2009]. Sixteen total periods were used in the inversion, for an inverted data array size of $55 \times 12 \times 16$. The model space dimension was $1400 \times 1400 \times 1001.79$ km and consisted of $106 \times 100 \times 74$ cells in the north (X), east (Y), and down (Z) directions, respectively. The smallest horizontal cell size was 0.3×0.3 km around the volcanic cones of Figure 1a; cell size increased with distance from the cones, to a maximum of 150×150 km. In the Z direction, grid spacing of a thickness of 1.79 km at elevations above sea level was finely set to account for topographic effects in the observed data. The thickness of 1.79 km was divided into 38 cells (grid spacing × the number of cells): 0.01 km × 3, 0.03 km × 4, 0.06 km × 25, 0.03 km × 4, and 0.01 km × 2 downward, which were determined based on a digital elevation model from the Geospatial Information Authority of Japan. Grid spacing below sea level was set to increase gradually from 10 m in the top layer to 300 km in the lowermost layer.

For the input resistivity model, all values were initialized to unfixed values of 80 Ω m for land, a fixed value of 0.33 Ω m for sea, and a fixed value of 100,000,000 Ω m for air. The model fit to the observed data was determined using the root-mean-square (RMS) misfit, $\mathrm{RMS} = \sqrt{\sum_{i=1}^{N} C_{d_i}^{-2} \left(d_i - F[m]_i\right)^2 / N}$, where N is parameter size ($55 \times 12 \times 16$), d is observed data, $F[m]$ is synthetic data (computed as the forward response of the optimum model, m), and C_d is the data error. The inversion continued until either reaching a predetermined maximum number of allowed iterations (in this study, 10) or a target RMS misfit (in this study, 1.0 ± 0.05).

We applied a two-step procedure to MT response functions in this inversion analysis. In the first step, we obtained a rough model by setting the error floors of the observed data to relatively large values. In the second step, a well-constrained final model was obtained by setting error floors to smaller values and using the rough model as a starting model. In the inversion code, the unconstrained function, which is used to seek the smoothest/minimum norm model for an appropriate fit to the observed data, is given by

$$U(\mathbf{m}, \quad \lambda) = \lambda^{-1}\left\{(\mathbf{d} - \mathbf{F}[\mathbf{m}])^T \mathbf{C_d}^{-1}(\mathbf{d} - \mathbf{F}[\mathbf{m}]) - \chi^2\right\} + (\mathbf{m} - \mathbf{m}_0)^T \mathbf{C_m}^{-1}(\mathbf{m} - \mathbf{m}_0), \tag{2}$$

where $\mathbf{m}$ is the optimum resistivity model of dimension M ($106 \times 100 \times 74$), λ^{-1} is a Lagrange multiplier, $\mathbf{d}$ is the observed data of dimension N, $\mathbf{F}[\mathbf{m}]$ is the forward response of the optimum model, $\mathbf{C_d}$ is the data covariance matrix, χ^2 is the target value of the RMS misfit, $\mathbf{m}_0$ is the prior model, $\mathbf{C_m}$ is the model covariance matrix, and the superscript T denotes the transpose operator [*Siripunvaraporn et al*., 2005; *Siripunvaraporn and Egbert*, 2009]. A fixed prior model, which is the same as the starting model, was used to constrain the solution during the inversion procedure. Error floors in the first step were set to 20% for MT impedance tensors and 30% for tipper vectors; in the second step, they were reduced to 5% for MT impedance tensors and 10% for tipper vectors.

We obtained RMS misfit values of 1.01 for the model of the first step and 2.09 for the final model of the second step. Figures 2 and S1 in the supporting information show the fit between observed and synthetic data for the final model: the fit in Figure 2 is based on sounding curves of the six MT response functions at three representative sites, and the fit in Figure S1 is based on the phase tensors of the MT impedance tensors in *Caldwell et al*. [2004] and the induction arrows of the tipper vectors in *Parkinson* [1962] at all sites for three periods. The fits of the off-diagonal components of the MT impedance tensors (Z_{XY} and Z_{YX}) indicate complete agreement, whereas the relative fits of the diagonal components (Z_{XX} and Z_{YY}) and tipper vectors (T_{ZX} and T_{ZY}) vary with respect to Z_{XY} and Z_{YX}. Based on quantitative and visual evaluation of observed and synthetic data for the final model by the RMS misfit value and the sounding curves, we conclude that the synthetic data give a good fit to the observed data overall.

3. Results and Discussion

Our three-dimensional electrical resistivity model clearly reveals an upwelling magma-like conductive anomaly, of which resistivity values show 1–40 Ω m, around the Naka-dake first crater. Incidentally, resistivity values of the upper crust beneath Aso caldera in the previous larger-scale resistivity model, which consisted of 5 km grid spacing in the Z direction for the upper crust, indicate that the most conductive blocks of 3 Ω m exist around the northwest of Naka-dake and the most resistive blocks of ~3000 Ω m exist around the southeast of the caldera [*Hata et al*., 2015]. Figures 3 and 4 show three horizontal cross sections at depths of 2–2.5, 6–7, and 9–10 km and six cross sections at depths of $<$20 km. Three of the cross sections (profiles A1, A2, and A3) are aligned N60°W–S60°E; the other three (B1, B2, and B3) are perpendicular to this direction. All profiles traverse the central volcanic cones across Aso caldera. Moreover, two profiles, A2 and B1, pass over the Naka-dake first crater. On all vertical and horizontal cross sections, earthquake hypocenters determined by the Japan Meteorological Agency (JMA) are plotted for two periods: June 2002 to December 2013 and January 2014 to April 2016.

3.1. Sensitivity Tests

We now examine whether the sensitivity of our inversion model is sufficient to resolve a series of conductive anomalies (C1 and C2 on profiles A1, A2, B1, and B2) through three-dimensional forward modeling. For this test, cells with resistivity values of $<$40 Ω m in anomaly C1 (at depths of 1.5–13 km, with a north-south length of 5.9 km and an east-west width of 3.3 km) were replaced by cells with resistivity values of 40 Ω m. A similar replacement procedure was applied to anomaly C2 (at depths of 0.04–3 km, with a north-south length of 2.4 km and an east-west width of 3.6 km), which seems to branch off from conductive anomaly C1 at depths of $<$5 km. Figure S2 shows representative cross sections of replaced blocks in the two sensitivity test models. RMS misfits for the sensitivity test models are 2.25 for C1 and 2.12 for C2; these are increases from the RMS misfit of the final model (2.09). Significant changes in MT response functions are found in the sounding curves of the off-diagonal impedance tensors (especially Z_{XY}); a representative example of this is shown in Figure S2. The synthetic sounding curves of the sensitivity test models depart from observed curves at long periods ($T >$ 10 s). Thus, the series of conductive anomalies appears to be a reliable feature.

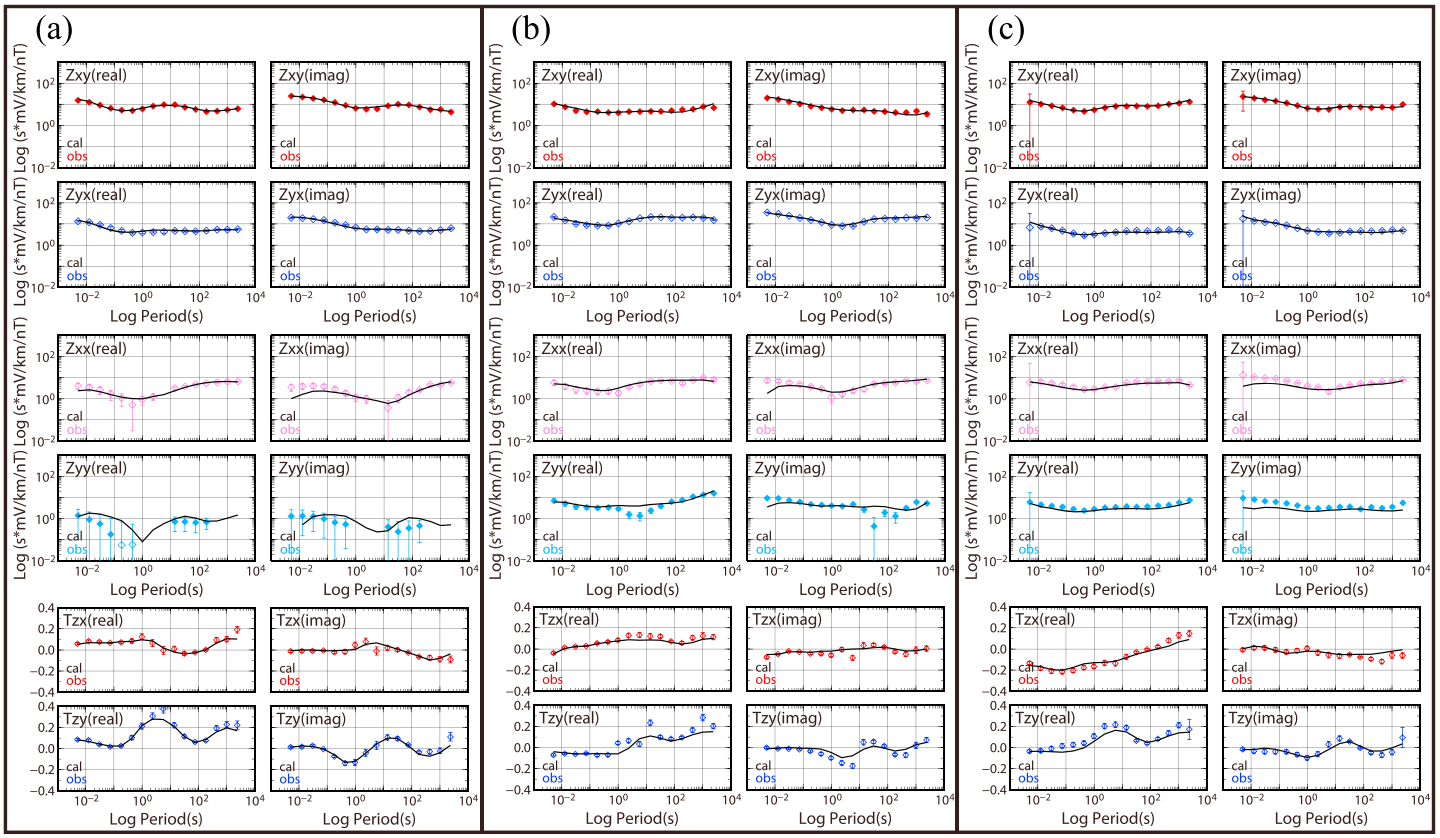

Figure 2. Sounding curves of the complex MT response functions (Z_{XX}, Z_{XY}, Z_{YX}, Z_{YY}, T_{ZX}, and T_{ZY}) for three representative sites (a, b, and c; Figure 1). Black lines and diamonds with error bars indicate synthetic and observed data, respectively. Solid and open diamonds represent positive and negative values for MT impedance tensors (Z_{XX}, Z_{XY}, Z_{YX}, and Z_{YY}), respectively.

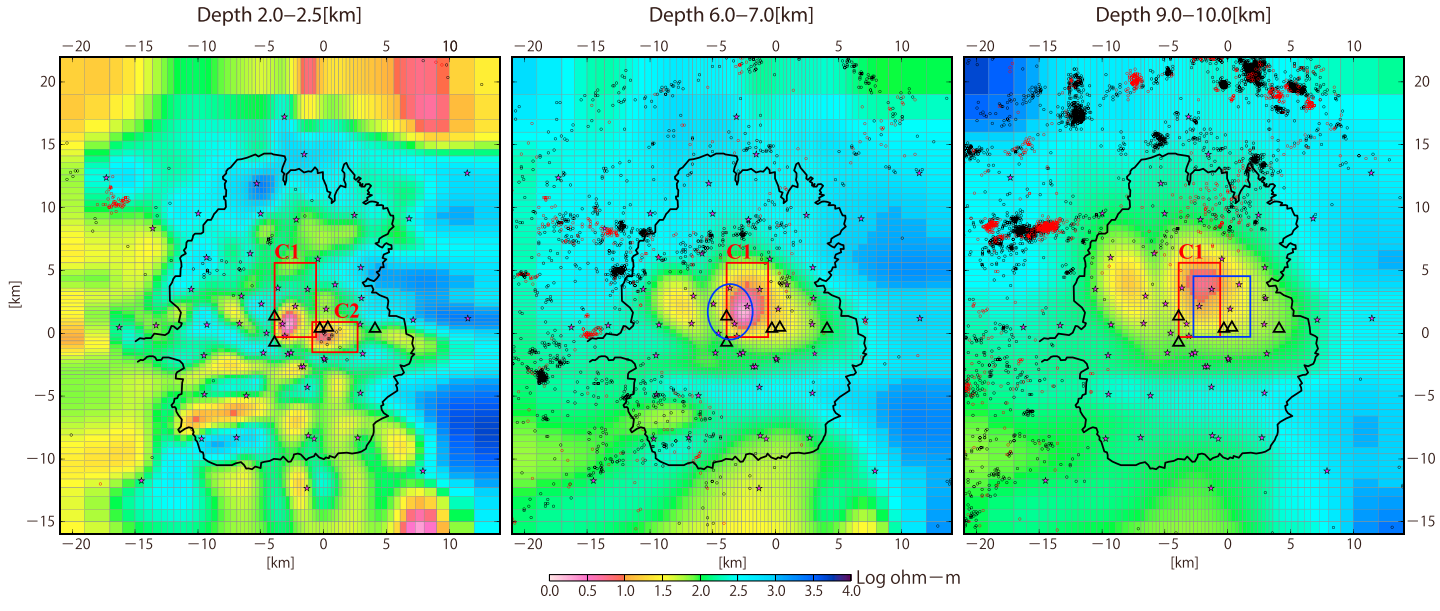

Figure 3. Horizontal cross sections of the electrical resistivity model at depths of 2.0–2.5, 6.0–7.0, and 9.0–10.0 km, with earthquake hypocenters determined by the Japan Meteorological Agency (JMA). Pink stars, black triangles, and black outline indicate MT sites, principal postcaldera cones, and the rim of Aso caldera, respectively. The blue rectangle and circle indicate the inferred sill-like deformation source at 15.5 km depth [*Geographical Survey Institute*, 2004] and spherical *P* velocity anomaly of $< -15\%$ at 6 km depth [*Sudo and Kong*, 2001], respectively. Earthquakes that occurred between June 2002 and December 2013 are represented by black dots; earthquakes from January 2014 to April 2016 are represented by red dots.

3.2. Imaged Electrical Resistivity Structure

The series of significant conductive block anomalies (C1 and C2), which extend in a northward direction as depth increases to about 15 km, can be seen on profiles A1, A2, B1, and B2 in the crust beneath Naka-dake. These anomalies can be regarded as an upwelling magma pathway and reservoir in the upper crust. We estimated melt fractions for the most conductive cell of the two conductive anomalies, 0.79 Ω m at a depth of 4 km for C1 and 5.6 Ω m at a depth of 2 km for C2. First, we calculated resistivity values of silicate melt using SIGMELTS [*Pommier and Le-Trong*, 2011] then calculated melt fractions based on the resistivity values using the Hashin-Shtrikman upper bound [*Hashin and Shtrikman*, 1962]. For obtaining the resistivity values of silicate melt beneath Naka-dake, we used the following results of chemical analyses of scoria samples ejected at November 2014 eruption: the averaged chemical composition of groundmass (Na_2O 3.26 wt % and SiO_2 58.62 wt %) and the temperature (1113°C ≈ 1386 K) and water content (1.0–2.0 wt.%) of magma based on melt inclusions (Geological Survey of Japan, 2015; G. Saito, personal communication, 2015). Besides these values, we adopted the general lithostatic pressure (109.76 MPa at a depth of 4 km for C1 and 54.88 MPa at a depth of 2 km for C2) using a continental crust density of 2800 kg/m^3 and the resistivity of surrounding material of 80 Ω m based on our final model. Finally, the resistivity values of silicate melt were estimated at 0.54–0.61 Ω m for C1 and 0.52–0.59 Ω m for C2, and the melt fractions were estimated at 76–87% for the most conductive cell of C1 and 13–14% for that of C2.

The magma pathway is considered a crucial factor in understanding volcanic activity at Naka-dake. The spatial extent of this series of conductive anomalies is highly consistent with the low-velocity anomaly resolved by *Sudo and Kong* [2001], and the conductive anomalies lie above the sill-like deformation source [*Geographical Survey Institute*, 2004]. Thus, there is a possibility that the location and extent of the magma reservoir have appeared and existed to be spatially stable for at least 15 years. Temporal patterns in earthquake clusters show little variation between the two periods mentioned above, despite the 15 year extent of the JMA seismic catalog (see Figures 3 and 4). Incidentally, a significant earthquake cluster, which we can see within the conductive anomaly C2 on profile A2, is distributed at depths of upper ~5 km. The earthquake cluster is considered to be triggered by pore pressure fluctuations associated with the magma. *Farquharson et al*. [2016] reported through stressing experiments on volcanic rock (porous andesite) that an increase of pore pressure can result in rock fracture even under a lithostatic pressure state and can assist in the development of fractured zones surrounding the conduit, and the rock embrittlement can create transient outgassing pathways by linking fracture networks. Moreover, quasi-horizontal conductive blocks at shallow depths (upper ~2 km) on all the cross sections are considered to mainly originate in altered rocks [e.g., *Kanda et al*., 2008].

Another significant feature is an apparent spatial correlation between earthquake hypocenters and resistive blocks on the north sides of the central volcanic cones. The hypocenters in the northwest are distributed at or inside the resistive blocks (profiles A1, A2, and A3; Figure 4). On the other hand, practically all of the hypocenters in the northeast are distributed at the resistive sides of the boundaries between resistive and conductive blocks (profiles B1, B2, and B3, Figure 4). The earthquakes in the northeast seem to occur at the resistive sides along the upper surface of the upwelling magma-like conductor. This suggests that the sides of resistive blocks can be subjected to stress concentrations related to the earthquakes. Research on the relative deviatoric stress field on Kyushu from the focal mechanisms of shallow earthquakes reported that the stress regime changes around Aso [e.g., *Matsumoto et al*., 2015]. Thus, our three-dimensional electrical resistivity model appears to detect subsurface variations in rock properties associated with the magma reservoir/pathway.

Comparison of our resistivity structure model with other resistivity structure models beneath subduction volcanoes with calderas is helpful to understanding the cause of spatial variations (conductive and resistive anomalies) in our resistivity structure model and the cause of spatial correlations between those anomalies and earthquake hypocenters. *Ogawa et al*. [2014] reported a vertical conductor, which extends to a depth of ~5 km from a greater depth, in the upper crust beneath Naruko volcano with late Miocene collapse calderas in the Northeastern Japan Arc. They also reported that a lower cutoff depth ($<$5 km) of the crustal seismicity distribution is consistent with the top of the conductor. And then, they suggested that the conductor originates in saline fluids supplied by a partial melting zone at a greater depth, and the fluid reservoir is capped by a self-sealed precipitate of silicate solution at the shallow depth of ~5 km. Taken together with seismological data, vertical conductive zones, which support a model of hydrothermal convection, are

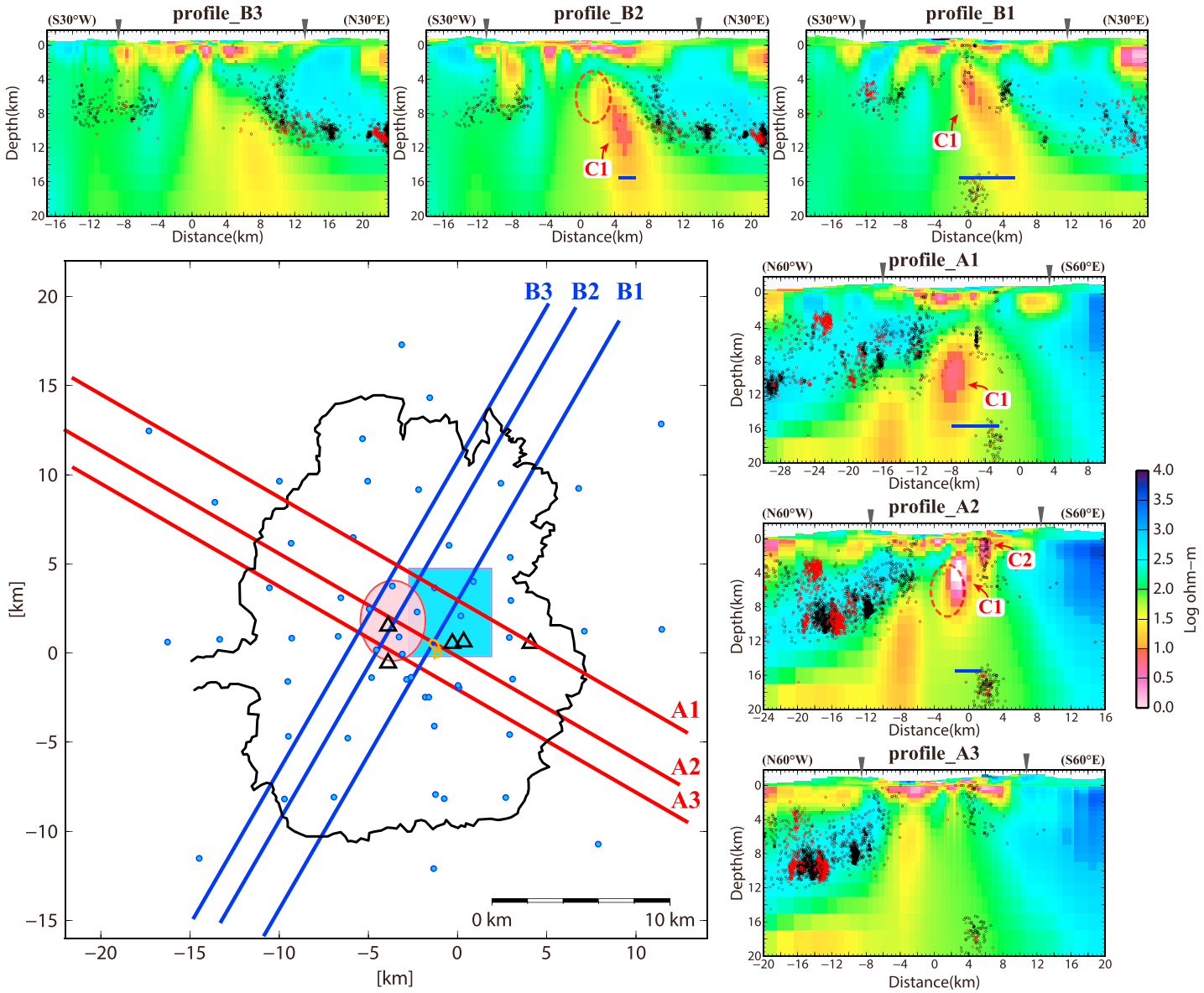

Figure 4. Cross sections of three-dimensional electrical resistivity along six profiles (A1–3 and B1–3). Blue dots, black triangles, orange outline, and black outline indicate MT sites, the five main postcaldera cones, Naka-dake first crater, and the rim of Aso caldera, respectively. The blue rectangle and red circle indicate the inferred sill-like deformation source at 15.5 km depth [*Geographical Survey Institute*, 2004] and spherical *P* velocity anomaly of $< -15\%$ at 6 km depth [*Sudo and Kong*, 2001]. JMA earthquake hypocenters within 2 km of each profile line are indicated on cross sections: black dots correspond to earthquakes between June 2002 and December 2013, and red dots correspond to earthquakes between January 2014 and April 2016. Gray triangles represent locations on the caldera rim. Blue lines at 15.5 km depth (on profiles A1, A2, B1, and B2) and red dashed line circles at 3–6 km depth (on profiles A2 and B2) indicate the sill-like deformation source and the spherical *P* velocity anomaly along each profile lines, respectively.

revealed within the brittle (upper ~6–7 km) part of the crust beneath the Taupo volcanic zone with collapsed calderas in New Zealand [*Bertrand et al.*, 2012]. Namely, these spatial variations of the resistivity structures in the crust beneath the subduction volcanoes are considered to be affected by not only magma (melt, aqueous fluids, gas, and solid) but also temperature.

For comparison, seismic tomography and waveform modeling studies have reported an upper crustal magma reservoir at depths of 5–17 km in the Yellowstone Caldera [e.g., *Chu et al.*, 2010; *Farrell et al.*, 2014]. *Farrell et al.* [2014] suggested that many of the extensive earthquake swarms in Yellowstone, which are distributed at the upper surface side of the magma reservoir, can be attributed to migrating magmatic fluids (hydrothermal fluids and CO_2-saturated gas) from the crustal magma reservoir. In the Long Valley Caldera,

local earthquake tomography and receiver function analysis have revealed two low-velocity anomalies: an elongate anomaly at a depth of 6 km and a broad anomaly at depths of 8–14 km beneath the caldera [*Seccia et al.*, 2011]. These low-velocity anomalies were also regarded as magma paths, in which the deep magma body fed partial melt to the shallow magma body.

4. Conclusions

We resolved three-dimensional electrical resistivity structure beneath Aso caldera, Japan, using magnetotelluric data with an array geometry designed to detect magma reservoirs. Our model reveals a possible magma pathway in the form of a significant series of conductive anomalies in the upper crust, extending north from Naka-dake cone at depths of >10 km. The center of these anomalies gradually shifts toward Naka-dake to the south, along with a decrease in anomaly depths. The melt fractions were estimated at 79–87% at the depth of 4 km and 13–15% at the depth of 2 km. Moreover, the inferred magma pathway is spatially correlated with earthquake hypocenters in and around Aso caldera during the past 15 years. Earthquakes occurred mainly on the north sides of volcanic cones in the central part of the caldera. Importantly, earthquake clusters occur within resistive blocks in the northwest but occur at the resistive sides of the boundaries between resistive blocks and conductive blocks (i.e., the inferred magma pathway) in the northeast. Thus, our electrical resistivity model resolves well-supported structures that can be attributed to a northward dipping magma pathway and/or reservoir beneath Aso caldera.

Acknowledgments

We thank all members of Aso Volcanological Laboratory, Kyoto University, Japan, for their assistance with observations. Special thanks are given to T. Uchide and M. Uyeshima for discussions relevant to this study. We would like to thank Y. Ogawa and P. Wannamaker for their careful review. This study was partly supported by the Secretariat of the Nuclear Regulation Authority, Japan. Figures were created using Generic Mapping Tools [*Wessel and Smith*, 1998]. All data are available for evaluating the contents of this paper; data can be requested by contacting M.H. (m.hata@aist.go.jp). All other data requests will be evaluated on a case-by-case basis because the data cannot be released to the public.

References

Abe, Y., T. Ohkura, K. Hirahara, T. Shibutani, K. Hirahara, and M. Kato (2010), Crustal structure beneath Aso Caldera, Southwest Japan, as derived from receiver function analysis, *J. Volcanol. Geotherm. Res.*, *195*, 1–12.

Bertrand, E. A., et al. (2012), Magnetotelluric imaging of upper-crustal convection plumes beneath the Taupo Volcanic Zone, New Zealand, *Geophys. Res. Lett.*, *39*, L02304, doi:10.1029/2011GL050177.

Cagniard, L. (1953), Basic theory of the magnetotelluric method of geophysical prospecting, *Geophysics*, *18*, 605–645.

Caldwell, T. G., H. M. Bibby, and C. Brown (2004), The magnetotelluric phase tensor, *Geophys. J. Int.*, *158*, 457–469.

Chu, R., D. V. Helmgerger, D. Sun, J. M. Jackson, and L. Zhu (2010), Mushy magma beneath Yellowstone, *Geophys. Res. Lett.*, *37*, L01306, doi:10.1029/2009GL041656.

Farquharson, J., M. J. Heap, P. Baud, T. Reuschlé, and N. R. Varley (2016), Pore pressure embrittlement in a volcanic edifice, *Bull. Volcanol.*, *78*, 6.

Farrell, J., R. B. Smith, S. Husen, and T. Diehl (2014), Tomography from 26 years of seismicity revealing that the spatial extends well beyond the Yellowstone caldera, *Geophys. Res. Lett.*, *41*, 3068–3073, doi:10.1002/2014GL059588.

Geographical Survey Institute (2004), Geographical Survey Institute Crustal deformations around Aso Volcano Report of Coordinating Committee for Prediction of Volcanic Eruption [in Japanese], No.88, 106–110.

Handa, S. (2005), Electrical conductivity structures estimated by thin sheet inversion, with special attention to the Beppu-Shimabara graben in central Kyushu, Japan, *Earth Planets Space*, *57*, 605–612.

Hase, H., T. Hashimoto, S. Sakanaka, W. Kanda, and Y. Tanaka (2005), Hydrothermal system beneath Aso volcano as inferred from self-potential mapping and resistivity structure, *J. Volcanol. Geotherm. Res.*, *143*, 259–277.

Hashin, Z., and S. Shtrikman (1962), A variational approach to the theory of effective magnetic permeability of multiphase materials, *J. Appl. Phys.*, *33*, 3125.

Hata, M., N. Oshiman, R. Yoshimura, Y. Tanaka, and M. Uyeshima (2015), Three-dimensional electromagnetic imaging of upwelling fluids in the Kyushu subduction zone, Japan, *J. Geophys. Res. Solid Earth*, *120*, 1–17, doi:10.1002/2014JB011336.

Hyndman, R. D., and P. J. Shearer (1989), Water in the lower continental crust: Modelling magnetotelluric and seismic reflection results, *Geophys. J. Int.*, *98*, 343–365.

Kanda, W., Y. Tanaka, M. Utsugi, S. Takakura, T. Hashimoto, and H. Inoue (2008), A preparation zone for volcanic explosions beneath Naka-dake crater, Aso volcano, as inferred from magnetotelluric surveys, *J. Volcanol. Geotherm. Res.*, *178*, 32–45.

Matsumoto, A., K. Uto, K. Ono, and K. Watanabe (1991), K-Ar age determinations for Aso volcanic rocks—Concordance with volcanostratigraphy and application to pyroclastic flows— [in Japanese], Abstracts Fall Meet. in 1991, Volcanol. Soc. Japan, 73.

Matsumoto, S., S. Nakao, T. Ohkura, M. Miyazaki, H. Shimizu, and Y. Abe (2015), Spatial heterogeneities in tectonic stress in Kyushu, Japan and their relation to a major shear zone, *Earth Planets Space*, *67*, 172.

Ogawa, Y., M. Ichiki, W. Kanda, M. Mishina, and K. Asamori (2014), Three-dimensional magnetotelluric imaging of crustal fluids and seismicity around Naruko volcano, NE Japan, *Earth Planets Space*, *66*(1), 158.

Ono, K., I. Matsumoto, M. Miyahisa, Y. Teraoka, and N. Kambe (1977), Geology of the Taketa district, with geological sheet map at 1:50,000 [in Japanese with English abstract], Geol. Surv. Japan, 145 pp.

Parkinson, W. D. (1962), The influence of continents and oceans on geomagnetic variations, *Geophys. J. Int.*, *6*, 441–449.

Pommier, A., and E. Le-Trong (2011), "SIGMELTS": A web portal for electrical conductivity calculations in geosciences, *C. R. Geosci.*, *37*, 14,501–459.

Seccia, D., C. Chiarabba, P. De Gori, I. Bianchi, and D. P. Hill (2011), Evidence for the contemporary magmatic system beneath Long Valley Caldera from local earthquake tomography and receiver function analysis, *J. Geophys. Res.*, *116*, B12314, doi:10.1029/2011JB008471.

Siripunvaraporn, W., and G. Egbert (2009), WSINV3DMT: Vertical magnetic field transfer function inversion and parallel implementation, *Phys. Earth Planet. Int.*, *173*(3–4), 317–329.

Siripunvaraporn, W., G. Egbert, Y. Lenbury, and M. Uyeshima (2005), Three-dimensional magnetotelluric inversion: Data-space method, *Phys. Earth Planet. Int.*, *150*, 3–14.

Sudo, Y. (2001), The character of volcanic activity at Aso volcano: An open system volcano [in Japanese], *Chikyu Mon.*, *23*, 545–550.

Sudo, Y., and L. S. L. Kong (2001), Three-dimensional seismic velocity structure beneath Aso Volcano, Kyushu, Japan, *Bull. Volcanol.*, *63*, 326–344.

Wessel, P., and W. H. F. Smith (1998), New improved version of generic mapping tools released, *EOS Trans. AGU*, *79*, 579.